Estuarine, Coastal and Shelf Science 279 (2022) 108134

Contents lists available at ScienceDirect

Estuarine, Coastal and Shelf Science

journal homepage: www.elsevier.com/locate/ecss

Seagrass distribution, areal cover, and changes (1990–2021) in coastal waters off West-Central Florida, USA

Luis Lizcano-Sandoval [a,*], Christopher Anastasiou [b], Enrique Montes [c,e], Gary Raulerson [d], Edward Sherwood [d], Frank E. Muller-Karger [a]

[a] College of Marine Science, University of South Florida, St. Petersburg, FL, United States
[b] Southwest Florida Water Management District, Tampa, FL, United States
[c] Ocean Chemistry and Ecosystems Division, NOAA Atlantic Oceanographic and Meteorological Laboratory, Miami, FL, United States
[d] Tampa Bay Estuary Program, St. Petersburg, FL, United States
[e] University of Miami Cooperative Institute for Marine & Atmospheric Studies, Miami, FL, United States

ARTICLE INFO

Keywords:
Seagrass
Remote sensing
Google earth engine
Landsat
Sentinel
Ecosystem monitoring

ABSTRACT

Seagrass meadows of West-Central Florida (USA), between 27°3′N – 28°12′N; 82°24′W – 82°50′W, are closely monitored by federal, state, and local groups for benthic composition, density, and areal cover (extent). Biennial aerial mapping, annual in situ surveys, and monthly water quality measurements inform management and conservation actions. Here we leverage a complete archive of multiple satellite imagery products (i.e., Landsat-5, Landsat-7, Landsat-8, and Sentinel-2 imaging sensor data) to reconstruct seagrass areal cover estimates (1990–2021) in four regions of West-Central Florida: St. Joseph Sound, Clearwater Harbor, Tampa Bay, and Sarasota Bay. Satellite imagery hosted in Google Earth Engine (GEE) was screened for low cloud cover (<40%), and clear atmosphere and water conditions using a semi-automated process followed by visual inspection. Imagery meeting these conditions for seagrass mapping was available for 16 years: 1990, 1992, 1996, 1999, 2000, 2004–2006, 2010, and 2015–2021. Space-based time series of seagrass areal cover for each region showed a positive correlation with estimates from aerial mapping ($r > 0.61$). Over the period 1990–2021, satellite-derived estimates show seagrass areal cover increased by 24.3 km^2 (34.4%) in Tampa Bay, 18.0 km^2 (74.1%) in St. Joseph Sound, 6.3 km^2 (182.6%) in Clearwater, and 1.3 km^2 (5.3%) in Sarasota. Overall, the combined seagrass areal cover for the entire region increased by 49.9 km^2 (40.6%), or ~1.4% yr^{-1}, from 1990 through 2021. Increases in seagrass areal cover before 2020 coincide with improvements in water quality throughout the region (i.e., a general decrease in chlorophyll-a, phosphorous, nitrogen concentration, and turbidity). The publicly-available satellite datasets in GEE provide resource managers with complementary and unique tools for synoptic and repeated seagrass areal cover assessments. This is an important approach to monitor the seagrass cover Essential Ocean Variable (EOV) of the Global Ocean Observing System (GOOS).

1. Introduction

Seagrasses are found in shallow coastal zones from the tropics to the sub-Arctic. They support diverse and productive biological communities and provide a wide range of benefits to humans (Duarte et al., 2005; Waycott et al., 2009). The ecological and biogeochemical role of seagrasses depends on local seagrass areal cover. While estimating global seagrass areal cover remains a challenge (McKenzie et al., 2020), many studies show a decline in local seagrass areal cover around the world. For example, Waycott et al. (2009) reported that seagrass areal cover in Australia, United States, and Europe declined about 1.5% yr^{-1} between 1879 and 2006. Sudo et al. (2021) estimated a loss of 4.7% yr^{-1} between 2000 and 2020 in Southeast Asia. Telesca et al. (2015) reported a decline of 34% in *Posidonia oceanica* areal cover using almost 50 years of data from the Mediterranean Sea, similar to the 29% decline reported by de los Santos et al. (2019) in European seagrasses between 1869 and 2016. Yet, many regions lack basic information on seagrass areal cover and are not routinely monitored.

Seagrass habitats off West-Central Florida have been mapped and monitored routinely using aerial photography and in-situ surveys for

* Corresponding author.
E-mail addresses: luislizcanos@usf.edu, carib@usf.edu (L. Lizcano-Sandoval), carib@usf.edu (F.E. Muller-Karger).

https://doi.org/10.1016/j.ecss.2022.108134
Received 9 March 2022; Received in revised form 15 September 2022; Accepted 26 October 2022
Available online 30 October 2022

many years. The Southwest Florida Water Management District (SWFWMD) has been conducting aerial mapping of seagrass habitats along Florida's Gulf coast since 1988. In-situ seagrass transect monitoring has been ongoing in the estuaries of Tampa Bay, Sarasota Bay, Lemon Bay, and Charlotte Harbor since early 1990s. These efforts are possible through state, regional, and local partnerships facilitated through the Tampa Bay Estuary Program (TBEP) and Florida Aquatic Preserves (Sherwood et al., 2016). The estuaries of West-Central Florida are generally dominated by three seagrass species: *Thalassia testudinum*, *Halodule wrightii*, and *Syringodium filiforme* (Yarbro and Carlson, 2016; Sherwood et al., 2017). Two more ephemeral species are also observed at much lower frequencies: *Ruppia maritima* and *Halophila engelmannii* (Sherwood et al., 2017).

In Tampa Bay, seagrass areal cover decreased 47% between 1950 and 1982 as urbanization expanded and water quality degraded (Lewis et al., 1985; Johansson and Lewis, 1992; Greening et al., 2014). The recognition that seagrasses are a critical habitat for fish and manatees in Tampa Bay led to an active campaign by the TBEP to manage nitrogen inputs into Tampa Bay (Greening et al., 2014). The goal was to improve the light availability for seagrasses by increasing water clarity through a reduction in water column chlorophyll concentration associated with phytoplankton biomass stimulated by nutrient inputs. Implementation of initiatives and projects based upon this paradigm have been successful over the past 30 years resulting in a recovery of seagrass areal cover to levels comparable to that of the 1950s and surpassing these estimates in 2016 at 416.5 km^2 (Johansson and Lewis, 1992; Tomasko et al., 2005, 2018; Greening et al., 2014; Sherwood et al., 2017; Beck et al., 2019). Seagrass beds in other regions off West-Central Florida such as Sarasota Bay have increased in cover by 32% over the period 1950–2016 (Tomasko et al., 2018). Regions such as St. Joseph Sound and Clearwater Harbor lack long-term seagrass monitoring data. However, over the period 1999–2016, seagrass bed cover in St. Joseph Sound and Clearwater Harbor increased by 10.5% and 43.7%, respectively (Tomasko et al., 2018).

Among the challenges in monitoring seagrass areal cover is the cost and time involved in conducting repeated aerial and in-situ surveys. Several studies have explored the potential of using satellite imagery to map seagrass habitats, since many different types of satellite data covering coastal areas of the world are openly available, such as Landsat and Sentinel missions (Lyons et al., 2013; Topouzelis et al., 2018; Traganos et al., 2018; Poursanidis et al., 2019; Veettil et al., 2020). Likewise, seagrass mapping efforts along the West-Central Florida coast have been attempted for St. Joseph Sound and Clearwater Harbor using imagery from Landsat-5, IKONOS, and Hyperion for 2003, 2005, 2006, 2009, and 2010 (Meyer and Pu, 2012; Pu et al., 2012, 2014; Pu and Bell, 2017).

Seagrass areas are typically identified in multispectral satellite data using spectral clustering algorithms. Machine learning classifiers, such as Classification and Random Tree (CART) and Random Forest, have been tested for seagrass mapping, but several studies find that Support Vector Machine (SVM) algorithms provide the best qualitative outputs with high accuracies (Marcello et al., 2018; Traganos and Reinartz, 2018; Traganos et al., 2018; Wicaksono et al., 2021). The SVM algorithm aims to find an optimal hyperplane that separates the dataset into a predefined number of classes that minimizes misclassifications (Mountrakis et al., 2011). As with most machine learning classifiers, seagrass mapping uncertainties tend to increase in areas with low seagrass density (Roelfsema et al., 2013, 2014). Furthermore, spatial and spectral resolution of satellite imagery can be insufficient to accurately identify and differentiate seagrass species from other submerged vegetation (Phinn et al., 2008).

Here we use imagery from the Landsat sensors and Sentinel-2 satellite series to further understand seagrass areal cover changes along West-Central Florida. We defined seagrass areal cover as extent of seagrass beds in an area. Our goals were to: 1) quantify changes of seagrass areal cover using Landsat-5, Landsat-7, Landsat-8, and Sentinel-2

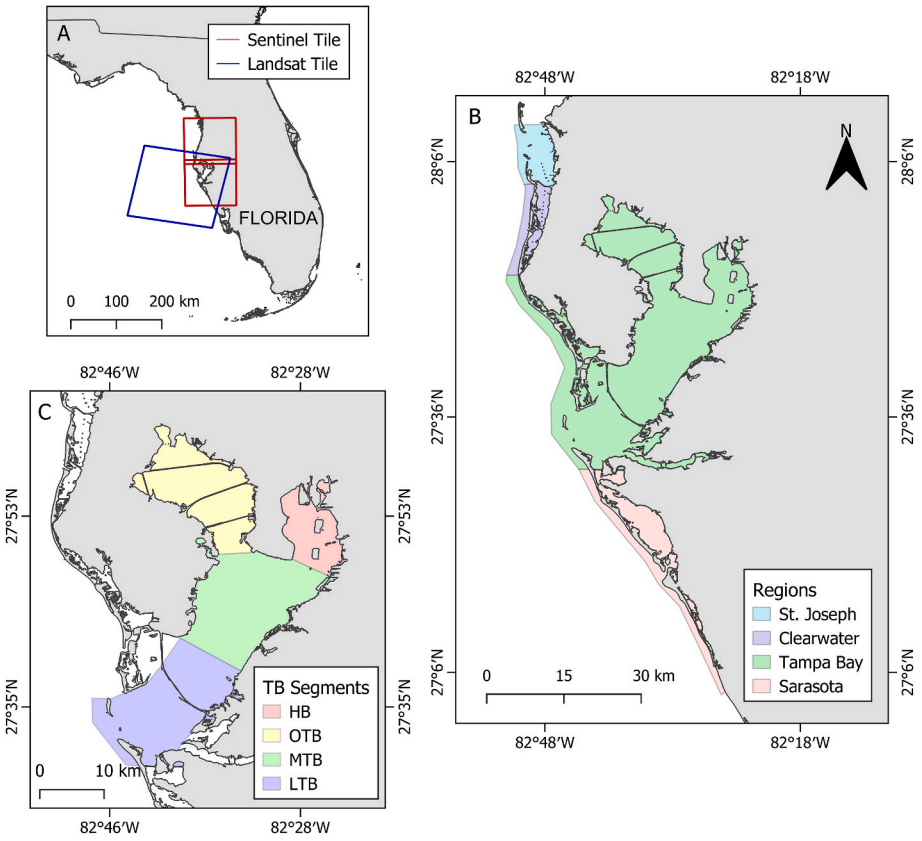

Fig. 1. Maps of the study area. (A) Outline of the tiles for repeated image scene selection: Two Sentinel-2 tiles and one Landsat tile used to cover the area of interest. (B) The four areas mapped off West-Central Florida: St. Joseph Sound, Clearwater Harbor, Tampa Bay, and Sarasota Bay. (C) Four major Tampa Bay segments studied: Hillsborough Bay (HB), Old Tampa Bay (OTB), Middle Tampa Bay (MTB), Lower Tampa Bay (LTB). The location of the monthly water quality stations from the Environmental Protection Commission of Hillsborough County (EPCHC) for each bay segment are also shown with color-coded dots. (For interpretation of the references to color in this figure legend, the reader is referred to the Web version of this article.)

imagery over 1990–early 2021 in four regions of West-Central Florida (Fig. 1: St. Joseph Sound, Clearwater Harbor, Tampa Bay, and Sarasota Bay), exploiting the potential of Google Earth Engine (GEE) for larger scale mapping in complex coastal waters; 2) validate the seagrass areal cover estimates using historical estimates derived from aerial surveys in those four regions; 3) evaluate seagrass areal cover trends in the context of water quality data within Tampa Bay; and 4) implement an open-access seagrass monitoring application using the GEE platform, and providing access to the historical satellite data in the cloud. This is an important approach to monitor the seagrass areal cover Essential Ocean Variable (EOV) of the Global Ocean Observing System (Miloslavich et al., 2018; Muller-Karger et al., 2018a, b).

2. Methods

2.1. Study area

We focused our study on St. Joseph Sound, Clearwater Harbor, Tampa Bay, and Sarasota Bay in West-Central Florida (Fig. 1). We considered the Sarasota Bay region as a group of Sarasota Bay and other smaller water bodies such as Roberts Bay, Little Sarasota Bay, and Blackburn Bay. In these estuaries, seagrass beds typically grow at depths of 2 m or shallower as described by monitoring data from the TBEP and SWFWMD. For resource management purposes, Tampa Bay has been further divided into four major segments: Hillsborough Bay (HB), Old Tampa Bay (OTB), Middle Tampa Bay (MTB), and Lower Tampa Bay (LTB). Water quality in Tampa Bay is driven by precipitation, rivers, urban and industrial discharges, and wind- and tidal nutrient and sediment sources. These also modulate the concentration of phytoplankton in the water column (Le et al., 2013). High precipitation typically occurs in June–September and low precipitation in October–May (Morrison et al., 2006). The highest and lowest levels in river discharge and chlorophyll concentration are observed in September and May, respectively (Chen et al., 2007; Le et al., 2013). Other factors such as winds and tides affect water quality in the bay through sediment resuspension during the dry season (Chen et al., 2007).

2.2. Satellite imagery

We used imagery from satellite sensors including Sentinel-2 (A and B), Landsat-8 Operational Land Imager (OLI), Landsat-7 Enhanced Thematic Mapper (ETM+), and Landsat-5 Thematic Mapper (TM) to cover an approximate study area of 3,611 km^2 for seagrass mapping in the regions of interest (Fig. 1). Differences between Sentinel-2 A/B sensors and Landsat sensors include spatial resolution, revisit time, and spectral bands (Table 1).

We identified imagery available between 1990 and early 2021. Seagrass was mapped for images characterized by good atmospheric conditions and good water visibility (e.g., no clouds and clear waters) (see Methods Section 2.3.1). Only the initial four years of Landsat-7 imagery were used because of the failure of the Scan Line Corrector in early 2003, which caused a strip pattern and data gaps in each image after that. Landsat-5 and Landsat-7 imagery overlapped between 1999 and 2003, allowing for a larger number of images for mapping in those years. A gap occurred in 2012 between the failure of Landsat-5 in mid-2012 and the launch of Landsat-8 in 2013. Landsat-8 imagery was not used jointly with Sentinel-2 imagery in overlapping years due to differences in pixel resolution between the sensors. Sentinel-2 was preferred for seagrass mapping after 2016, because of the faster revisit time afforded by two Sentinel-2 satellites (A and B) and better spatial resolution (Table 1).

Table 1
Characteristics of satellite sensors and relevant bands considered for seagrass mapping.

Satellite Sensor	Spatial Resolution (m)	Bands of Interest (nm)	Period Covered in this Study	Revisit Time (Days)
Landsat-5 TM	30	485, 560, 660	1984–2012	16
Landsat-7 ETM+	30	485, 560, 660	1999–2021	16
Landsat-8 OLI	30	443, 482, 561, 655	2013–2021	16
Sentinel-2A/B MSI	10	443[a], 482, 561, 655	2015–2021	~5

[a] Native resolution at 60 m resolution, but reprojected to 10 m.

All imagery was accessed through GEE. This is a cloud-based platform that offers easy access to multi-petabyte satellite imagery while also providing high-performance computing resources to process the data (Gorelick et al., 2017).

2.3. Processing workflow

The seagrass mapping workflow followed the four steps described below (Fig. 2).

2.3.1. Selection of images (Fig. 2I)

Satellite imagery was initially selected based on region of interest, cloud cover (<40%), and time of collection (years). For regions of interest, one tile was selected for Landsat and two tiles for Sentinel (Fig. 1). Images represent georeferenced, calibrated top-of-atmosphere radiance. Cloud and land masks (Section 2.3.2) were applied to each image. Only pixels within polygons defined for each region of interest were analyzed (Fig. 1B).

We used the normalized difference turbidity index (NDTI) to select images that contained the clearest water possible. The NDTI uses the red and green band ratios as a proxy for water turbidity in inland waters (Lacaux et al., 2007; Elhag et al., 2019), and it was useful also to identify good quality images for seagrass mapping in coastal shallow waters. The highest NDTI values observed (closer to zero) indicated images with turbid waters, sun glint, or unmasked clouds, while the lowest NDTI values (usually the most negative values) indicated images with best atmospheric and water conditions for the specific set of images and region of interest (Fig. 3). We calculated mean NDTI values and number of valid pixels per image, after masking land and clouds (Fig. 2). The best images for seagrass mapping were selected by inspecting the images with lowest NDTI mean values. Threshold values were not used since NDTI varied according to the area of interest, bottom features contributing to the NDTI (e.g., shallow seagrass beds and tidal flats), number of valid pixels after masking, and image quality. Most of the selected images were collected between January–March and October–December (Table S1). Restricting the analysis to this period also minimized any seasonal variation in seagrass cover that may affect the estimations.

2.3.2. Pre-processing (Fig. 2.II)

Top-of-atmosphere reflectance images from Sentinel and Landsat were converted to bottom-of-atmosphere (BOA) reflectance using the Py6S model, a 6S radiative transfer model coded in the Python programming language (Wilson, 2013). The code was adapted and modified from Sam Murphy (https://github.com/samsammurphy/gee-atmcorr-S2) to work with the respective satellite imagery using the GEE Python API (Appendix A). This allowed the same atmospheric correction to be applied across different satellite sensors in the cloud. The algorithm for cloud masking was modified from the Google cloudScore algorithm adapted by Chastain et al. (2019) and Poortinga et al. (2019) to work with Sentinel-2 and Landsat imagery. The cloudScore algorithm was modified to remove cold and bright pixels such as clouds and pixels with sun glint. We derived a high-resolution land mask of the region using the Normalized Difference Water Index (NDWI) algorithm with a few selected Sentinel-2 images (i.e. 10 m per pixel) (McFeeters, 1996). This index uses the green and near-infrared (NIR) bands to differentiate water from land.

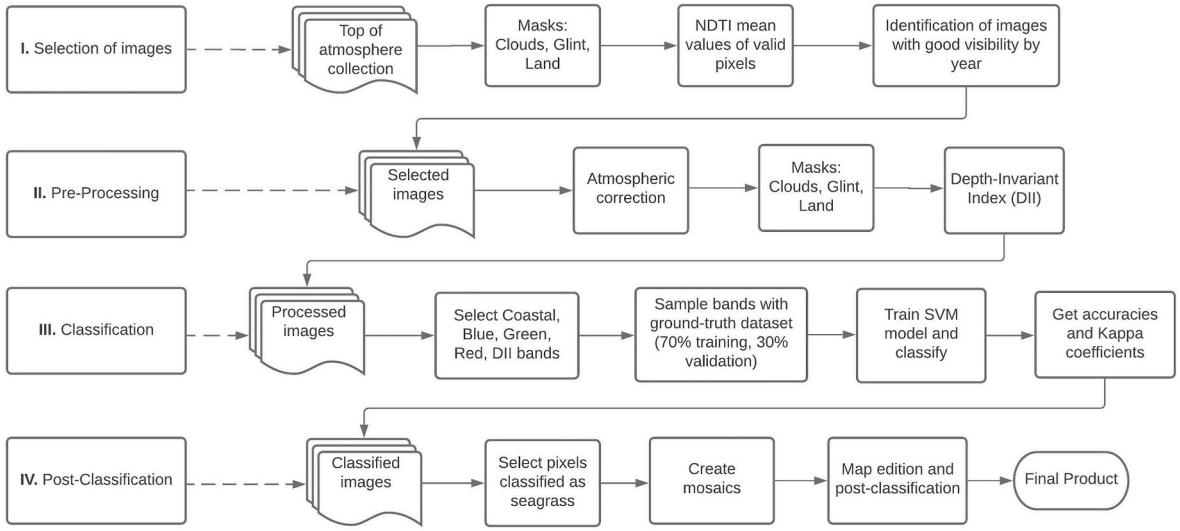

Fig. 2. Seagrass mapping workflow using Google Earth Engine. NDTI is the normalized difference turbidity index.

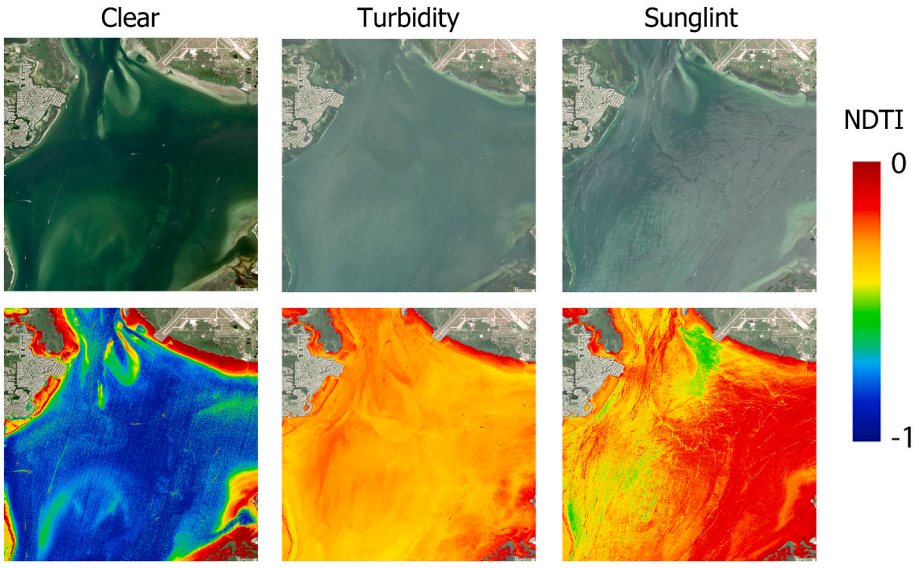

Fig. 3. Normalized difference turbidity index (NDTI) in Sentinel-2 images with synoptical clear waters, turbidity, and sunglint. Note the contribution of shallow seagrass beds and tidal flats to the NDTI.

Water column and bottom reflectance contribution to BOA reflectance in optically-shallow waters was corrected using the depth-invariant index (DII) method (Lyzenga, 1981; Green et al., 2000). Applying this method, spectral band ratios of the same bottom types (e.g., sand) across a depth gradient are linearized to compensate for light attenuation. The output of the blue and green band ratios was used as an additional input for seagrass classification (i.e., the DII band; see Section 2.3.3).

2.3.3. *Classification (Fig. 2.III)*

We compiled an initial ground-truthing dataset of 5,019 georeferenced points based on seagrass distribution from: 1) peer-reviewed publications (Table S2), 2) publicly-accessible databases (Beck, 2020; SWFWMD (https://data-swfwmd.opendata.arcgis.com)), and 3) interpretation of 2019 Sentinel-2 satellite imagery (10 m resolution) and aerial imagery (1 m resolution) from the National Agriculture Imagery Program (NAIP), as accessed from GEE. Point data were distributed into *softbottom* (N = 2,584), *hardbottom* (N = 185), and *seagrass* (N = 2,250). The *hardbottom* and *softbottom* categories span a variety of non-vegetated benthic substrates including rocks, sand, and mud.

The total number of ground-truth points available was 3,054 for tile 17RLM and 2,142 for tile 17RLL (both for Sentinel-2), and 2,558 for tile 017/041 (path/row for Landsat). The available points were randomly assigned to training (70%) and validation (30%) datasets. The spatial distribution and number of points of this initial ground-truth dataset changed depending on year and valid pixels after masking (Table 2). The ground-truth datasets for other years before and after 2019 were built by adding or deleting points of the initial dataset as required, according to known seagrass distribution and visual interpretation of satellite imagery for each year. A link to the baseline dataset is provided in Appendix B.

Input for training of the SVM classification algorithm included available bands within the visible spectra of Landsat and Sentinel satellite sensors: the coastal aerosol (if available), blue, green, and red bands; in addition to the DII band. The use of the spectral bands along with the DII is intended to increase multidimensionality and classification accuracy of SVM, as described by Zhang et al. (2006), and to compensate for the effect of shallow water column on bottom

Table 2
Seagrass mapping accuracies and Kappa coefficients per year (mean ± standard deviation).

Year	Satellite	Number of Images	Average Ground-Truth Points	Accuracy (%)	Kappa
1990	Landsat-5	2	2,348	79.6 ± 6.9	0.64 ± 0.10
1992	Landsat-5	2	2,681	77.2 ± 1.8	0.59 ± 0.07
1996	Landsat-5	3	2,545	84.4 ± 3.2	0.72 ± 0.02
1999	Landsat-5	3	2,655	73.6 ± 3.1	0.59 ± 0.11
2000	Landsat-5/7	4	2,662	80.9 ± 2.6	0.67 ± 0.05
2004	Landsat-5	2	2,609	79.5 ± 5.8	0.68 ± 0.07
2005	Landsat-5	3	2,629	80.4 ± 3.5	0.64 ± 0.07
2006	Landsat-5	3	2,576	81.1 ± 1.7	0.67 ± 0.04
2010	Landsat-5	3	2,600	74.1 ± 3.8	0.56 ± 0.04
2015	Landsat-8	3	2,478	78.3 ± 5.5	0.58 ± 0.10
2016	Sentinel-2	8	2,382	84.0 ± 4.4	0.67 ± 0.06
2017	Sentinel-2	7	2,368	85.2 ± 5.8	0.67 ± 0.08
2018	Sentinel-2	6	2,272	83.5 ± 5.0	0.67 ± 0.08
2019	Sentinel-2	8	2,445	87.9 ± 4.1	0.78 ± 0.06
2020	Sentinel-2	7	2,394	86.4 ± 6.0	0.76 ± 0.09
2021	Sentinel-2	4	2,450	85.0 ± 2.6	0.70 ± 0.05

reflectance (Section 2.3.1). However, the benefit of including the DII band was not measured in this study, since this is a typical procedure for benthic mapping. The SVM classifier was tuned using the RBF kernel with gamma and cost values set as 100. SVM classifier accuracies were assessed using the respective validation dataset using "producer accuracy" for seagrass pixels and Kappa statistics of the overall classification (Congalton and Green, 2009). The producer accuracy is the number of sample units (i.e., pixels) classified as seagrass divided by the number of sample units indicated as seagrass (i.e., ground truth points). The Kappa statistic measures the agreement between the remotely sensed classification and reference data in an error matrix. The Kappa values range from +1 to −1, where values < 0.4 indicate poor agreement, values between 0.4 and 0.75 indicates good agreement, and values > 0.75 indicate a strong agreement (Kalkhan et al., 1997). The seagrass classification algorithm is provided in Appendix C. The classification was performed image by image, and not on image composites as is often done in benthic mapping studies.

2.3.4. *Post-classification (Fig. 2.IV)*

Pixels classified as seagrass in individual images were grouped to create one mosaic per year. A criterion to reduce misclassification errors was to keep only those seagrass pixels that appeared in the same location in at least 50% of the images (Fig. 4). This method was carefully adapted to each mosaic per tile, region, and year. Maximum seagrass pixel restriction was avoided (i.e., retention of seagrass pixels present in all classified images) when possible, to reduce the loss of true seagrass pixels identified in certain images (Fig. 4B). However, in cases with only two images per year this criterion did not apply, and the images were mosaicked without conditions. The raster mosaic was manually edited in post-processing to mask out or to include pixels that may have included seagrass based on ground-truth and airborne observations according to visual interpretations. For example, segments like OTB and HB required more attention due to the presence of the attached green algae *Caulerpa* spp. Between 2017 and 2021, shifts from seagrass to *Caulerpa* have been

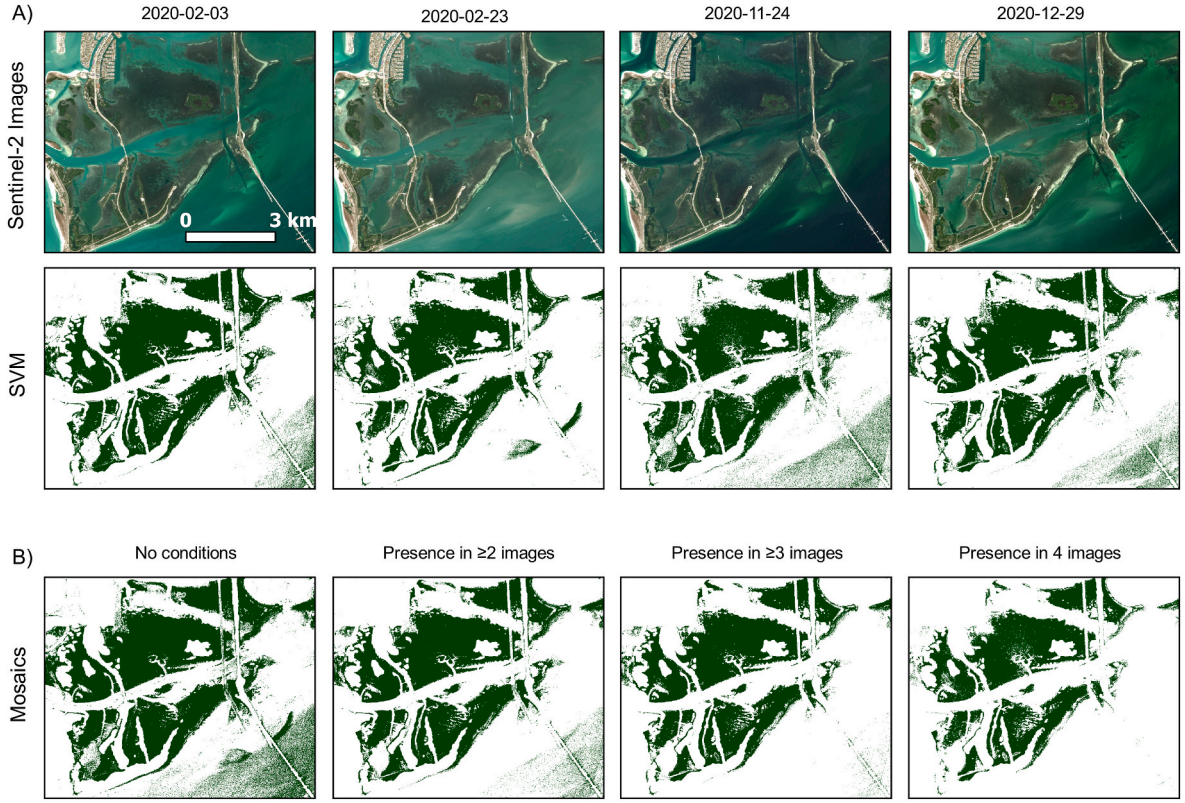

Fig. 4. Seagrass classification in different Sentinel-2 images using the SVM classifier (A) and after applying mosaicking conditions of seagrass presence according to the number of classified images per year. Note the reduction of misclassified pixels in the lower right corner of the mosaics as seagrass pixel restriction increases.

observed by TBEP in annual transect monitoring (Beck, 2020). Deep water and areas of no interest were manually masked out. This editing helps to increase the reliability of final seagrass maps, especially for time-series mapping consistency. The seagrass maps are provided in Appendix B.

2.4. Analyses

Seagrass maps produced from Landsat imagery were re-gridded to 10 m to allow a pixel-by-pixel comparison to Sentinel-2 seagrass products, e.g., 1990's Landsat map vs. 2021's Sentinel-2 map. This type of pixel-by-pixel spatial comparison was not possible with the SWFWMD vector file products. The classification accuracies of each classified image were averaged per year as an indicator of image and classification qualities of mosaicked seagrass maps.

The benthic classification by the SWFWMD using aerial photographs includes two seagrass categories: continuous and patchy (Sherwood et al., 2017; Anastasiou and Morton, 2021a, b). Available seagrass areas estimated were only extracted from the continuous seagrass category at each region due to this category being the most dominant, and similar and comparable to quantification of areal cover of dense seagrass beds by satellite remote sensing.

Time series of seagrass areal cover obtained with satellite and aerial imagery were compared. When an annual estimate from either dataset was not available, we filled the gap using a linear interpolation of these estimates between nearest years. A comparison among seagrass areas of 2020 estimated with Landsat-8, Sentinel-2, and aerial photography was used to estimate variability across the different products and methodologies. Differences in seagrass areal cover estimated by satellite imagery in 1990 and 2021 were calculated for each region and Tampa Bay segment. The rate of change in areal cover (% yr^{-1}) was obtained from the regression slope of the respective time series data.

Additional assessments of seagrass cover change and long-term water quality monitoring data was only performed in Tampa Bay due to a lack of consistent dataset in the other estuaries (Fig. 1C). Water quality indicators such as chlorophyll-a, total nitrogen, phosphorus, dissolved oxygen concentration, turbidity, temperature, and salinity were downloaded from the Tampa Bay Water Atlas (https://www.tampabay.wateratlas.usf.edu/). The monthly data collected by the Environmental Protection Commission of Hillsborough County (EPCHC) at 45 stations within Tampa Bay (Fig. 1C) were averaged annually for each bay segment over the period 1990–2020. Water quality trends over time were quantified. We used the Akaike's Information Criterion (AIC) method with stepwise selection to find the water quality variables that contribute the most to an optimal model of seagrass areal cover variability in each Tampa Bay segment, using satellite estimates. A multiple linear regression (MLR) was performed using the variables selected by the AIC.

Most of the workflow steps were done using the GEE web platform and GEE Python API. The post-classification was done with GEE and Serval plugins in QGIS v3.16, which was used for satellite imagery visualization and raster edition. The descriptive statistics and plots were made in Python. The AIC and MLR were performed with the Fathom toolbox for Matlab. Links to the atmospheric correction and seagrass classification codes are provided in the Appendix section. A link to the GEE app developed for examination of seagrass changes among years is also provided in Appendix D.

3. Results

Satellite-derived seagrass maps were generated for 16 years between 1990 and 2021 (Table 2). In total, 68 out of 926 images were determined to be useful for processing (Table S1). The seagrass mapping accuracies and Kappa statistics derived from aggregated Landsat and Sentinel products ranged from 73.6% to 87.9% and from 0.56 to 0.78 over the period, respectively (Table 2). In general, accuracy of seagrass mapping was greater for Sentinel-2 imagery (83.5–87.9%) compared to Landsat products (73.6–84.4%).

The seagrass areal cover estimated by satellite remote sensing showed similar trends as those derived by SWFWMD (Fig. 5). The satellite-derived and SWFWMD time series were positively correlated for all regions ($r > 0.61$). The highest correlations were found for Tampa Bay ($r > 0.89$), which had the longest time series. The trends in all regions showed an overall increase in seagrass areal cover over the last 30 years (see Table S3 for values of data in Fig. 5).

Major changes in seagrass areal cover estimated using satellite imagery were identified for the periods 1990–2010 (+59.4%), 2010–2015 (−15.4%), and 2015–2021 (+29.2%) in St. Joseph Sound; 1990–2004 (+201.5%), 2004–2015 (−27.8%), 2015–2021 (+29.8%) in Clearwater Harbor; 1992–2000 (−16%) and 2000–2021 (+50.1%) in Tampa Bay; and 1990–2018 (+30%) and 2018–2021 (−19%) in Sarasota Bay. Declines were observed between 2018 and 2020 in all regions except St. Joseph Sound. This was followed by an increase in early 2021 in all regions with the exception of Sarasota Bay. The decline in Sarasota Bay since 2018 has led to slightly higher seagrass areal cover in 2021 than that estimated in the 1990's (+5.3% or 1.3 km^2) (Fig. 6). In contrast, Clearwater Harbor showed the highest increase in seagrass areal cover (+182.6% or 6.3 km^2) in relation to the period 1990–2021, followed by St. Joseph Sound (+74.1% or 18 km^2), and Tampa Bay (+34.4% or 24.3 km^2). For all areas off West-Central Florida combined, seagrass areal cover increased by 49.9 km^2 (40.6%) in the period 1990–2021 (Fig. 6). This represents an annual rate of 1.3% yr^{-1} over the 1990–2021 period.

We further examined differences in seagrass areal cover estimates from Sentinel-2 and Landsat-8 using data from 2020 (Fig. 7). Five images from 2020 for Landsat-8 were used for this specific comparison (Table S1). Specifically, seagrass areal cover estimates with Sentinel-2 were larger than those from Landsat-8 by +7.6% in St. Joseph Sound, +20.3% in Clearwater, +4.3% in Tampa Bay, and +1.4% in Sarasota Bay. On average, the difference between the Sentinel-2 and Landsat-8 products was +5.4%. Areal cover estimates derived from SWFWMD datasets were different from Sentinel-2 and Landsat-8 products. The respective difference was +5.1% and +11.7% in St. Joseph Sound, +31.9% and +43.4% in Clearwater Harbor, −2.9% and +1.3% in Tampa Bay, and 19.2% and 20.3% in Sarasota Bay (Fig. 7). The overall difference across regions was +5.7% (Sentinel-2) and +10.5% (Landsat-8). Seagrass maps showed similar distribution patterns among products, but some seagrass patches, edges, and other details were lost with coarser pixel resolution (Fig. 5B). The largest percent differences occurred in areas with the smallest seagrass areal cover (i.e., Clearwater Harbor and Sarasota Bay).

The change in seagrass areal cover derived using satellite imagery between 1990 and 2021 was +4.7% yr^{-1} in Clearwater, +2.19% yr^{-1} in St. Joseph Sound, +1.29% yr^{-1} in Tampa Bay, and +0.47% yr^{-1} in Sarasota. In Tampa Bay, rates were +7.87% yr^{-1} in HB, +2.31% yr^{-1} in OTB, +1.17% yr^{-1} in LTB, and +1.06% yr^{-1} in MTB. Seagrass rates of change in Tampa Bay were higher with water quality improvements in the most polluted segments over 1990–2020 (Table 3, Fig. 8). Tampa Bay segments showed a clear gradient of physical and chemical parameters (Table 3). During the period 1990–2020 were observed declines in chlorophyll-a, nitrogen, phosphorus, turbidity, salinity, and dissolved oxygen; and increases in surface temperature (Table 3). Decreasing trends of nitrogen, phosphorous, turbidity, and dissolved oxygen were significant ($p < 0.05$) (Table 3).

Declines in salinity were recorded in 1998 and 2003 in all segments (Fig. 8). An apparent increase in water temperature is observed after 2010, and lower mean values were occasionally recorded for OTB over 1990–2020. Dissolved oxygen was notably different between HB and OTB after 2010. Maximum concentrations in chlorophyll-a were recorded in 1994, 1995 and 1998. Nitrogen concentrations were higher in 1994 and 2000. Phosphorus concentrations were in constant decline since 1990, but occasional increases were recorded in 1998, 2004 and 2020. The major periods of change in seagrass areal cover in Tampa Bay,

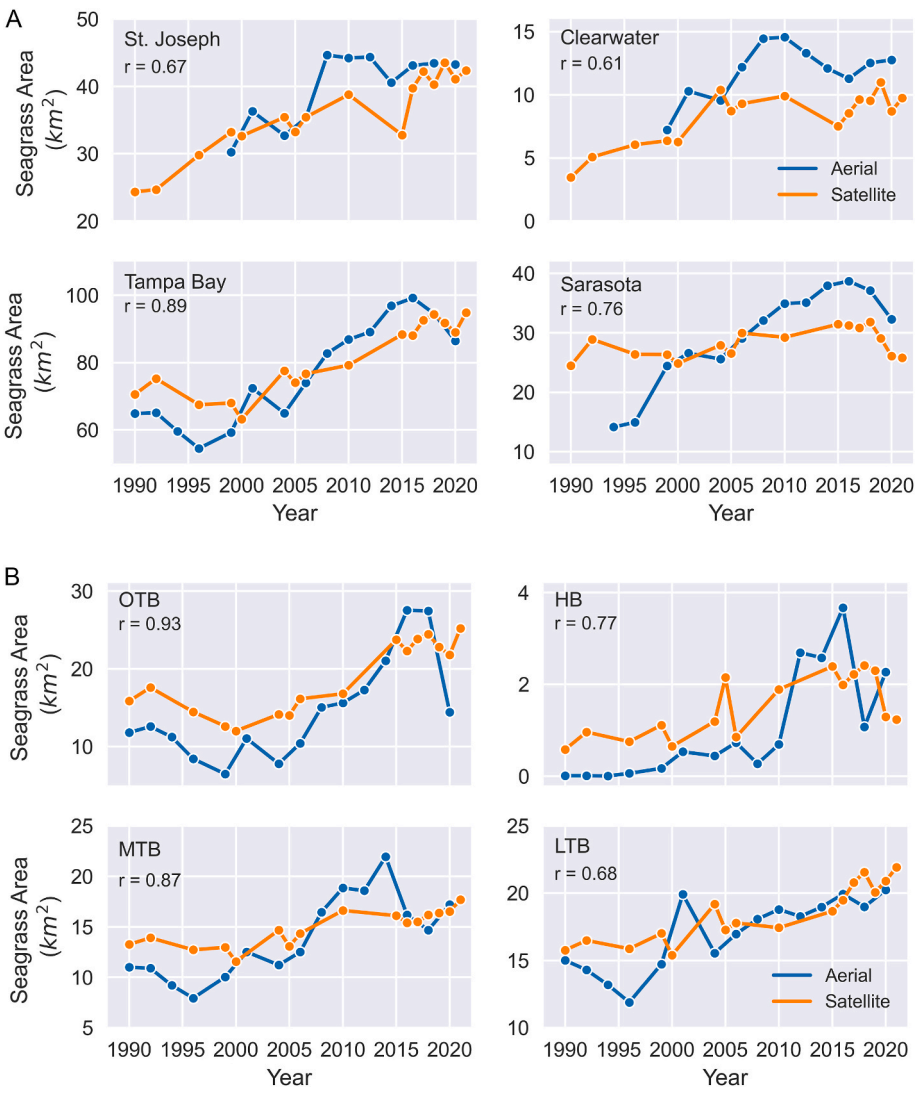

Fig. 5. Seagrass areal cover from 1990 to 2021 in several West-Central Florida regions (A) and within specific Tampa Bay segments (B) estimated from satellite imagery and aerial photography (SWFWMD). Correlation coefficients (r) between satellite and aerial time series are shown in each panel.

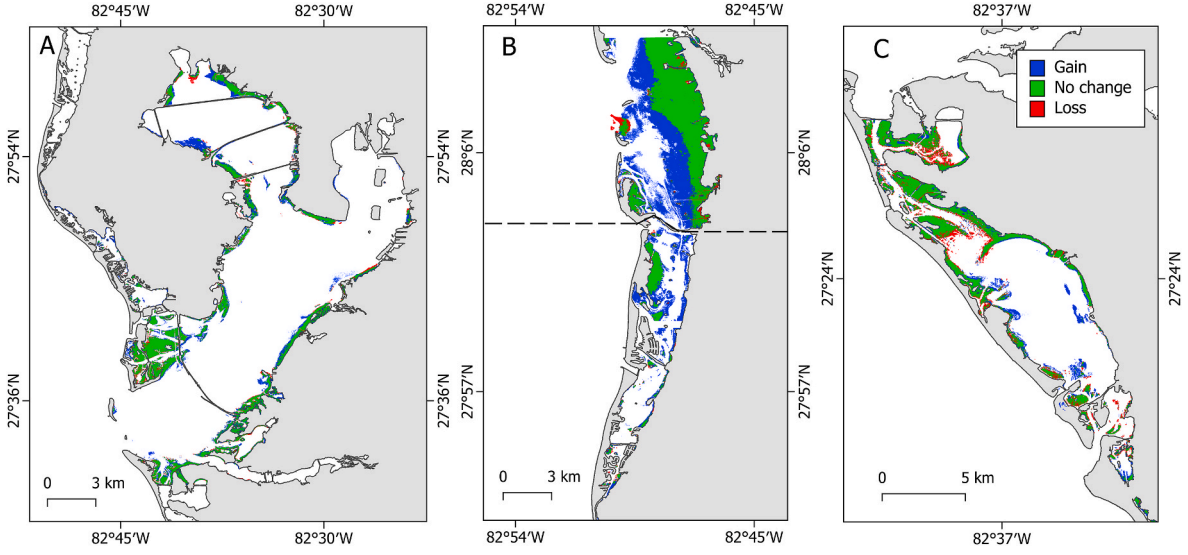

Fig. 6. Seagrass areal cover changes over the period 1990–2021 in (A) Tampa Bay, (B) St. Joseph Sound (upper half), Clearwater (lower half), and (C) Sarasota Bay, estimated with satellite mapping.

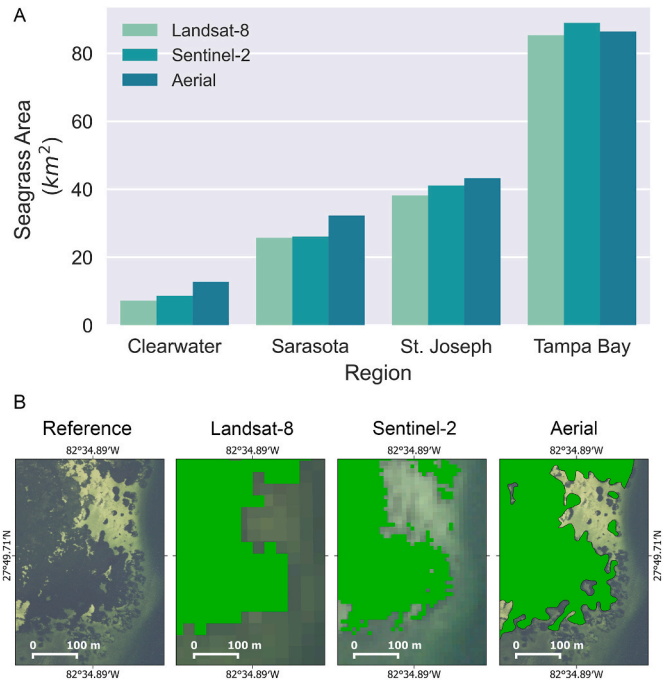

Fig. 7. Seagrass areas estimated with Landsat-8, Sentinel-2, and aerial photography in 2020. (A) Quantitative comparisons between products in four regions of West-Central Florida. (B) Comparison of seagrass cover maps produced by satellite imagery in this study and aerial photography by the SWFWMD.

before and after 2000, coincided with these contrasting water quality conditions over the same periods.

The water quality parameters that better explained changes in seagrass cover change during 1990–2020 were turbidity and total nitrogen in HB and OTB, turbidity and dissolved oxygen in MTB, and turbidity in LTB (Table S4). These parameters explained between 62 and 90% of the variability in seagrass areal cover change in Tampa Bay with a significance of $p < 0.05$ (Table 4).

4. Discussion

4.1. Ecological and management implications

Seagrass mapping products derived from satellite imagery and aerial mapping between 1990 and 2021 showed similar positive trends in estimates of seagrass areal cover. Legislation and regulation of wastewater and stormwater discharges beginning in the 1970s, and the establishment of national estuary programs in southwest Florida have supported the recovery of seagrass beds (Greening and Janicki, 2006; Sherwood et al., 2016; Tomasko et al., 2018). This led to enhanced fish production and ecosystem stability (Greening et al., 2014; Schrandt et al., 2021). In 2014, the goal to restore Tampa Bay seagrass areal cover to that in the 1950s was met (i.e., >153.78 km^2, including both continuous and patchy seagrass beds) (Sherwood et al., 2017).

Tampa Bay segments show differences in water quality that affect the rate of seagrass areal cover and distribution change over the studied period. Water quality changes in all Tampa Bay segments presented similar patterns over time at different levels and concentrations, especially in concentration of chlorophyll-a, total nitrogen, and phosphorous, and in turbidity and salinity. The most polluted segments (HB and OTB) showed larger increasing rates of seagrass areal cover than less polluted segments (MTB and LTB). This may represent a recovery response associated to water quality changes at different contamination levels. River discharge plays a major role in the water quality of Tampa Bay. Le et al. (2013) described positive correlations (>0.73) between river discharge and remotely sensed chlorophyll-a between 1998 and 2010 in Tampa Bay. They reported maximal water discharges for Alafia River, Hillsborough River, Little Manatee River, and Manatee River in 1998, 2003 and 2004, which coincided with minima in salinity and maxima in phosphorus and chlorophyll. Finer-scale assessments of observed water quality improvements across these segments of Tampa Bay relative to seagrass areal cover changes is needed to fully understand seasonal and interannual impacts on in seagrass distribution, cover, and health.

4.2. Seagrass mapping limitations

Seagrass mapping with remote sensing is possible only for shallow environments due to light attenuation with water depth. Poursanidis et al. (2019) were able to detect seagrass beds with Sentinel-2 imagery up to 32 m depth in oligotrophic waters of the Mediterranean. This is likely an extreme case, given the very clear water in some of the regions they studied. Such conditions are more limited off the West Florida coast, where tannic river discharges and estuarine production significantly obstruct water clarity. Variations in seagrass densities, water depth, turbidity, color, and pixel resolution impose additional limitations for seagrass mapping. We found that satellite remote sensing was able to detect seagrass patches larger than 100 m^2 for Sentinel-2 imagery and 900 m^2 for Landsat imagery, given their respective pixel resolutions. For each sensor, reflectance due to seagrass diminishes compared to other substrates as seagrass cover or density decrease within a pixel. Zoffoli et al. (2020) showed how the density of *Zostera noltei* may affect

Table 3
Changes in water quality in four Tampa Bay segments in the period 1990–2020. Regression slope values in bold are significative ($p < 0.05$).

Segments	Chl-a (mg m^{-3})	N (mg m^{-3})	P (mg m^{-3})	Turbidity (NTU)	Temperature (°C)	Salinity	Dissolved Oxygen (mg L^{-1})
	Mean ± S.D.						
HB	12.2 ± 3.0	614.5 ± 208.8	293.8 ± 91.1	5.0 ± 2.0	24.6 ± 0.6	24.7 ± 2.7	6.4 ± 0.4
OTB	9.6 ± 1.6	610.5 ± 206.7	182.9 ± 71.4	4.1 ± 1.4	24.0 ± 0.7	24.0 ± 3.0	6.6 ± 0.2
MTB	6.6 ± 1.5	506.9 ± 196.6	180.7 ± 60.8	3.5 ± 1.5	24.4 ± 0.5	27.3 ± 2.2	6.4 ± 0.2
LTB	4.2 ± 0.9	420.8 ± 164.3	100.5 ± 40.7	3.5 ± 1.5	24.3 ± 0.5	31.8 ± 1.4	6.4 ± 0.2
	Δ 1990–2020 (%)						
HB	−21.7	−51.0	−48.4	−72.9	0.5	−14.4	−4.0
OTB	0.5	−39.9	−33.6	−65.9	1.8	−21.2	−4.7
MTB	−32.8	−51.6	−33.7	−73.0	−0.1	−17.2	−3.6
LTB	−38.4	−40.7	122.1	−67.8	1.6	−13.8	−3.2
	Regression slope (in respective units)						
HB	−0.09	**−18.20**	**−7.36**	**−0.18**	0.01	−0.07	**−0.03**
OTB	0.04	**−16.62**	**−4.50**	**−0.12**	0.02	−0.10	**−0.01**
MTB	**−0.07**	**−15.78**	**−4.42**	**−0.14**	0.01	−0.06	**−0.02**
LTB	−0.03	**−10.30**	0.54	**−0.12**	0.02	−0.04	**−0.02**

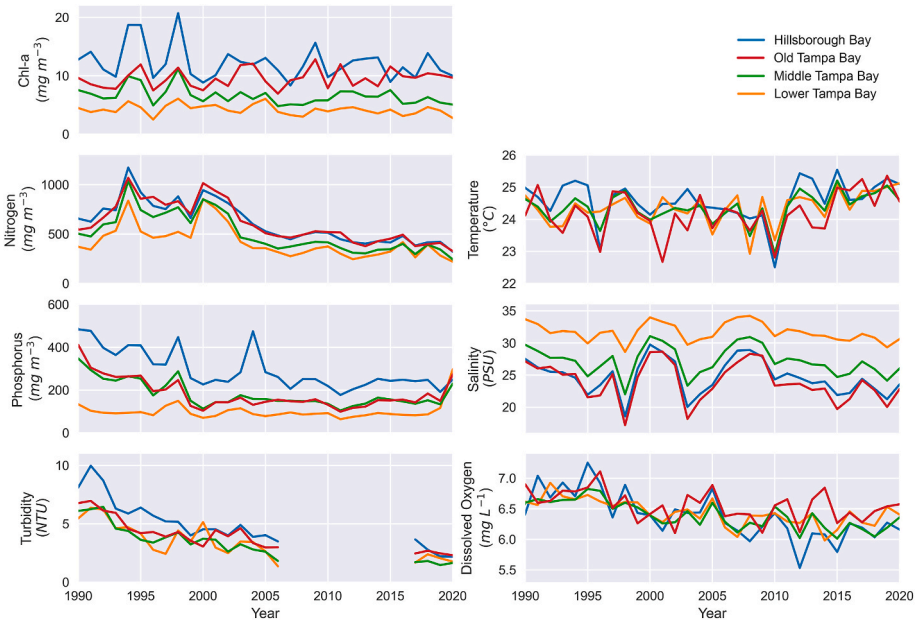

Fig. 8. Annual averages of water quality indicators at four major Tampa Bay segments monitored by the EPCHC. No turbidity data was available between 2007 and 2016.

Table 4
Multiple linear regression including the most significant water quality parameters contributing to seagrass areal cover change in each Tampa Bay segment.

Segment	Optimal Model	R^2	R^2-adj	F	p
HB	2007.13–5.66 x (Turbidity) - 4.84 x (Nitrogen)	0.88	0.86	42.98	0.001
OTB	2007.13–7.02 x (Turbidity) - 4.67 x (Nitrogen)	0.91	0.90	62.38	0.001
MTB	2007.13–6.86 x (Turbidity) - 3.50 x (DO)	0.86	0.83	35.79	0.001
LTB	2007.13–8.19 x (Turbidity)	0.65	0.62	23.96	0.001

its reflectance signature and increase mapping uncertainties in pixel areas with less than 50% of seagrass density. This demonstrates the limitation for seagrass mapping in areas with low seagrass densities.

Although depth was not a limitation in this study (seagrasses in the regions studied typically occur in <5 m depth), water quality and pixel resolution made it difficult to map some areas during rainy seasons. Our mapping methodology is applicable to shallow waters with presence of dense seagrass beds, mainly. Applications for mapping in deeper areas, with different satellite sensors, or seagrass species or densities may increase inaccuracies. The probability of misclassifications increases with depth, and some bottom features such as submerged vegetation and brown mud are indistinguishable below 10 m depth (Lyzenga, 1978). The capability to discriminate among seagrass species is also very limited and decreases with depth, and spectral and spatial resolution of the satellite images. For example, Phinn et al. (2008) mapped seagrass species shallower than 3 m in Australia with low to moderate producer accuracies (7–67%) using Quickbird-2 multispectral imagery at 2.4 m per pixel and low-high producer accuracies (8–84%) using CASI-2 hyperspectral imagery at 4 m per pixel. They were unable to map seagrass species using Landsat-5 imagery. Previous studies, datasets, and expert feedback are all important to improve mapping accuracy (Roelfsema et al., 2021).

4.3. Time-series mapping performance

Differences in classification accuracies (Table 2) and estimated areal cover between Landsat and Sentinel-2 imagery were observed (Fig. 7). The number and quality of the images used for seagrass mapping per year are important to accurately classify benthic habitats. Kovacs et al. (2018) found similar seagrass mapping accuracies but some differences in seagrass distribution patterns in maps produced with Landsat-8 at 30 m, Sentinel-2 at 10 m, ZY-3A at 5 m, and WorldView-3 at 2 m, in ~100 km^2 of seagrass beds in Moreton Bay, Australia. They also found similar seagrass areal cover derived with Landsat-8 and Sentinel-2, but ZY-3A and WorldView-3 provided lower seagrass areal cover estimates. In our study, we found that the seagrass areal cover in Clearwater Harbor estimated with satellite data from 2020 was <10 km^2, but that estimated with Sentinel-2 imagery was ~20% larger than that derived with Landsat-8. The Tampa Bay, Sarasota Bay, and St. Joseph Sound regions with seagrass areal cover >20 km^2 and <100 km^2 presented differences between 1.4% and 7.6% in calculated seagrass areas with Landsat-8 and Sentinel-2 in 2020. Differences with the estimates from the SWFWMD were expected due to mapping techniques, number of benthic classification classes, and human error. Nonetheless, we found similar trends of seagrass areal cover change and demonstrated the consistency of satellite mapping for estimating seagrass areal cover over time in West Florida.

The amount and quality of Sentinel-2 images compared to other satellite data increases the opportunities to map seagrasses at different times of the year in optically-complex coastal waters. Sentinel-2A and Sentinel-2B provided roughly three (3) times more data per year than individual Landsat satellites. Seagrass mapping efforts using annual Landsat-5 and Landsat-7 data from 1988 to 2010 have been successful in locations with low runoff impact in Australia (Lyons et al., 2013). However, seagrass mapping with Landsat becomes limited due to the lower historical availability of images for most coastal regions outside the United States (Wulder et al., 2016). Greater availability of images also allows monitoring of seasonal changes in benthic cover (Lyons et al., 2013; Wicaksono et al., 2021). Our seagrass mapping methodology explored the potential of GEE for increasing the mapping effort and create annual mosaics from individual classified images at larger spatial scales than traditionally pursued. Further studies on seagrass seasonality might be feasible in regions with complex water quality dynamics using combinations of several different satellite datasets and detailed in-situ data. Satellite-derived seagrass maps can support management efforts by detecting rapid changes in seagrass areal cover at faster and low-cost ways than the traditional methods. As such, these methods are recommended for use at larger temporal and spatial scales.

5. Conclusions

Repeated seagrass mapping contributes to understanding seagrass dynamics and changes over time. Mapping of seagrass habitat areal cover over large spatial and temporal scales is possible using satellite images and results are comparable to those from traditional aerial mapping methods. The West-Central Florida seagrass beds have increased their cover over the last three decades. Over 1990–2021, significant increases in seagrass cover were observed in Clearwater Harbor (182.6%), St. Joseph Sound (74.1%), and Tampa Bay (34.4%). Seagrass beds in Sarasota Bay have increased (5.3%), but continuous declines after 2018 were recorded and require more observation. Likewise, the upper Tampa Bay segments have experienced recent declines. Management actions by federal, state, and local groups to improve water quality in Tampa Bay have helped to effectively restore seagrass beds in the long-term. Tampa Bay segments with the highest concentrations in chlorophyll-a, nitrogen, phosphorus, and turbidity displayed the highest increases in seagrass areal cover as response to water quality improvements over time. Monitoring of seagrass areal cover over large areas is now possible and feasible with public satellite imagery available in the cloud, leveraging the high computing performance and large satellite imagery catalogs available in GEE. Cloud-computing mapping of seagrass beds using public satellite data provides a low-cost solution in assessing seasonal to interannual changes in areal cover of this critical habitat. It also complements information gathered from traditional survey methods, while also optimizing the use of field monitoring resources and adaptative management capacity of resource managers. These new cloud computing methods provide an important pathway to monitor the seagrass areal cover EOV over regional and eventually global scales.

CRediT authorship contribution statement

Luis Lizcano-Sandoval: Writing – original draft, Visualization, Methodology, Investigation, Funding acquisition, Formal analysis, Conceptualization. **Christopher Anastasiou:** Writing – review & editing, Resources. **Enrique Montes:** Writing – review & editing, Supervision. **Gary Raulerson:** Writing – review & editing, Resources. **Edward Sherwood:** Writing – review & editing, Resources. **Frank E. Muller-Karger:** Writing – review & editing, Supervision, Funding acquisition, Conceptualization.

Declaration of competing interest

The authors declare that they have no known competing financial interests or personal relationships that could have appeared to influence the work reported in this paper.

Data availability

Data will be made available on request.

Acknowledgements

This work was supported by the Marine Biodiversity Observation Network (MBON) grant from NASA (NNX14AP62A) and NOAA IOOS (NA19NOS0120199) under the National Ocean Partnership Program (NOPP RFP NOAA–NOS–IOSS-2014-2003803), the Gulf of Mexico Coastal Ocean Observing System (GCOOS/IOOS Cooperative Agreement NA16NOS0120018), and NSF (grant 1762493: Spokes: MEDIUM: SOUTH: Collaborative: Enhanced 3-D Mapping for Habitat, Biodiversity, and Flood Hazard Assessments of Coastal and Wetland Areas of the Southern US). This study was also supported by NASA under the A.50 AmeriGEO Work Programme of the Group on Earth Observations with grant number 80NSSC18K0318 ('Laying the foundations of the Pole-to-Pole Marine Biodiversity Observation Network of the Americas [MBON Pole to Pole]'). Special thanks to Fulbright, Colciencias, and the College of Marine Science at USF for supporting the doctoral studies and research of L. Lizcano-Sandoval with the Fulbright-Colciencias Scholarship, Norman Blake Endowed Memorial Fellowship, and Sanibel-Captiva Shell Club/Mary & Al Bridell Memorial Fellowship. We thank TBEP and local partners, SWFWMD, Tampa Bay Water Atlas, and EPCHC for providing seagrass and water quality monitoring data. We also thank Google Earth Engine for providing computing resources, geospatial analysis tools, and satellite data. We also thank Chuanmin Hu, Brigitta van Tussenbroek, and Susan Bell for their comments and guidance on satellite remote sensing and seagrass ecology during the initial preparation of this manuscript.

Supplementary data

Supplementary data to this article can be found online at https://doi.org/10.1016/j.ecss.2022.108134.

References

Anastasiou, C., Morton, N., 2021a. Final Report for the Seagrass Distribution from Tarpon Springs to Boca Grande – SWFWMD Seagrass 2020, Manual Photo-Interpretation. St. Petersburg, Florida, USA.

Anastasiou, C., Morton, N., 2021b. Photo-interpretation Key of Seagrass Distribution from Tarpon Springs to Boca Grande – SWFWMD Seagrass 2020. St. Petersburg, Florida, USA.

Beck, M.W., 2020. Tbep-Tech/Seagrasstransect-Dash: v1.0. https://doi.org/10.5281/zenodo.5507336.

Beck, M.W., Sherwood, E.T., Henkel, J.R., Dorans, K., Ireland, K., Varela, P., 2019. Assessment of the cumulative effects of restoration activities on water quality in Tampa Bay, Florida. Estuar. Coast 42, 1774–1791. https://doi.org/10.1007/s12237-019-00619-w.

Chastain, R., Housman, I., Goldstein, J., Finco, M., 2019. Empirical cross sensor comparison of Sentinel-2A and 2B MSI, Landsat-8 OLI, and Landsat-7 ETM+ top of atmosphere spectral characteristics over the conterminous United States. Remote Sens. Environ. 221, 274–285. https://doi.org/10.1016/j.rse.2018.11.012.

Chen, Z., Muller-Karger, F.E., Hu, C., 2007. Remote sensing of water clarity in Tampa Bay. Remote Sens. Environ. 109, 249–259. https://doi.org/10.1016/j.rse.2007.01.002.

Congalton, R.G., Green, K., 2009. Assessing the Accuracy of Remotely Sensed Data: Principles and Practices, second ed. CRC Press, Boca Raton, Florida, USA.

de los Santos, C.B., Krause-Jensen, D., Alcoverro, T., Marbà, N., Duarte, C.M., van Katwijk, M.M., Pérez, M., Romero, J., Sánchez-Lizaso, J.L., Roca, G., Jankowska, E., Pérez-Lloréns, J.L., Fournier, J., Montefalcone, M., Pergent, G., Ruiz, J.M., Cabaço, S., Cook, K., Wilkes, R.J., Moy, F.E., Trayter, G.M.R., Arañó, X.S., de Jong, D.J., Fernández-Torquemada, Y., Auby, I., Vergara, J.J., Santos, R., 2019. Recent trend reversal for declining European seagrass meadows. Nat. Commun. 10, 1–8. https://doi.org/10.1038/s41467-019-11340-4.

Duarte, C.M., Middelburg, J.J., Caraco, N., 2005. Major role of marine vegetation on the oceanic carbon cycle. Biogeosciences 2, 1–8. https://doi.org/10.5194/bg-2-1-2005.

Elhag, M., Gitas, I., Othman, A., Bahrawi, J., Gikas, P., 2019. Assessment of water quality parameters using temporal remote sensing spectral reflectance in arid environments. Saudi Arabia. Water 11, 556. https://doi.org/10.3390/w11030556.

Gorelick, N., Hancher, M., Dixon, M., Ilyushchenko, S., Thau, D., Moore, R., 2017. Google Earth engine: planetary-scale geospatial analysis for everyone. Remote Sens. Environ. 202, 18–27. https://doi.org/10.1016/j.rse.2017.06.031.

Green, E.P., Mumby, P.J., Edwards, A.J., Clark, C.D., 2000. Remote Sensing Handbook for Tropical Coastal Management. UNESCO, Paris, France.

Greening, H., Janicki, A., 2006. Toward reversal of eutrophic conditions in a subtropical estuary: water quality and seagrass response to nitrogen loading reductions in Tampa Bay, Florida, USA. Environ. Manag. 38, 163–178. https://doi.org/10.1007/s00267-005-0079-4.

Greening, H., Janicki, A., Sherwood, E.T., Pribble, R., Johansson, J.O.R., 2014. Ecosystem responses to long-term nutrient management in an urban estuary: Tampa Bay, Florida, USA. Estuar. Coast Shelf Sci. 151, A1–A16. https://doi.org/10.1016/j.ecss.2014.10.003.

Johansson, J.O.R., Lewis, R.R., 1992. Recent improvements of water quality and biological indicators in Hillsborough Bay, a highly impacted subdivision of Tampa Bay, Florida, USA. In: Marine Coastal Eutrophication: Proceedings of an International Conference. Elsevier, Bologna, Italy, pp. 1199–1215.

Kalkhan, M.A., Reich, R.M., Czaplewski, R.L., 1997. Variance estimates and confidence intervals for the Kappa measure of classification accuracy. Can. J. Rem. Sens. 23, 210–216. https://doi.org/10.1080/07038992.1997.10855203.

Kovacs, E., Roelfsema, C., Lyons, M., Zhao, S., Phinn, S., 2018. Seagrass habitat mapping: how do Landsat 8 OLI, Sentinel-2, ZY-3A, and Worldview-3 perform? Remote Sens Lett 9, 686–695. https://doi.org/10.1080/2150704x.2018.1468101.

Lacaux, J.P., Tourre, Y.M., Vignolles, C., Ndione, J.A., Lafaye, M., 2007. Classification of ponds from high-spatial resolution remote sensing: application to Rift Valley Fever epidemics in Senegal. Remote Sens. Environ. 106, 66–74. https://doi.org/10.1016/j.rse.2006.07.012.

Le, C., Hu, C., English, D., Cannizzaro, J., Kovach, C., 2013. Climate-driven chlorophyll-a changes in a turbid estuary: observations from satellites and implications for management. Remote Sens. Environ. 130, 11–24. https://doi.org/10.1016/j.rse.2012.11.011.

Lewis, R.R., Haddad, K.D., Johansson, J.O.R., 1985. Recent areal expansion of seagrass meadows in Tampa Bay, Florida: real bay improvement or drought-induced?. In: Tampa Bay Area Scientific Information Symposium. Tampa, FL, USA, pp. 189–192.

Lyons, M.B., Roelfsema, C.M., Phinn, S.R., 2013. Towards understanding temporal and spatial dynamics of seagrass landscapes using time-series remote sensing. Estuar. Coast Shelf Sci. 120, 42–53. https://doi.org/10.1016/j.ecss.2013.01.015.

Lyzenga, D.R., 1978. Passive remote sensing techniques for mapping water depth and bottom features. Appl. Opt. 17, 379. https://doi.org/10.1364/ao.17.000379.

Lyzenga, D.R., 1981. Remote sensing of bottom reflectance and water attenuation parameters in shallow water using aircraft and Landsat data. Int. J. Rem. Sens. 2, 71–82. https://doi.org/10.1080/01431168108948342.

Marcello, J., Eugenio, F., Martín, J., Marqués, F., 2018. Seabed mapping in coastal shallow waters using high resolution multispectral and hyperspectral imagery. Rem. Sens. https://doi.org/10.3390/rs10081208.

McFeeters, S.K., 1996. The use of the Normalized Difference Water Index (NDWI) in the delineation of open water features. Int. J. Rem. Sens. 17, 1425–1432. https://doi.org/10.1080/01431169608948714.

McKenzie, L.J., Nordlund, L.M., Jones, B.L., Cullen-Unsworth, L.C., Roelfsema, C., Unsworth, R.K.F., 2020. The global distribution of seagrass meadows. Environ. Res. Lett. 15, 074041 https://doi.org/10.1088/1748-9326/ab7d06.

Meyer, C.A., Pu, R., 2012. Seagrass resource assessment using remote sensing methods in St. Joseph Sound and Clearwater Harbor, Florida, USA. Environ. Monit. Assess. 184, 1131–1143. https://doi.org/10.1007/s10661-011-2028-4.

Miloslavich, P., Bax, N.J., Simmons, S.E., Klein, E., Appeltans, W., Aburto-Oropeza, O., Andersen Garcia, M., Batten, S.D., Benedetti-Cecchi, L., Checkley, D.M., Chiba, S., Duffy, J.E., Dunn, D.C., Fischer, A., Gunn, J., Kudela, R., Marsac, F., Muller-Karger, F.E., Obura, D., Shin, Y.J., 2018. Essential ocean variables for global sustained observations of biodiversity and ecosystem changes. Global Change Biol. 24, 2416–2433. https://doi.org/10.1111/gcb.14108.

Morrison, G., Sherwood, E.T., Boler, R., Barron, J., 2006. Variations in water clarity and chlorophyll a in Tampa Bay, Florida, in response to annual rainfall, 1985-2004. Estuar. Coast 29, 926–931. https://doi.org/10.1007/BF02798652.

Mountrakis, G., Im, J., Ogole, C., 2011. Support vector machines in remote sensing: a review. ISPRS J. Photogrammetry Remote Sens. 66, 247–259. https://doi.org/10.1016/j.isprsjprs.2010.11.001.

Muller-Karger, F.E., Miloslavich, P., Bax, N.J., Simmons, S., Costello, M.J., Sousa Pinto, I., Canonico, G., Turner, W., Gill, M., Montes, E., Best, B.D., Pearlman, J., Halpin, P., Dunn, D., Benson, A., Martin, C.S., Weatherdon, L.V., Appeltans, W., Provoost, P., Klein, E., Kelble, C.R., Miller, R.J., Chavez, F.P., Iken, K., Chiba, S., Obura, D., Navarro, L.M., Pereira, H.M., Allain, V., Batten, S., Benedetti-Checchi, L., Duffy, J.E., Kudela, R.M., Rebelo, L.-M., Shin, Y., Geller, G., 2018a. Advancing marine biological observations and data requirements of the complementary Essential Ocean Variables (EOVs) and Essential Biodiversity Variables (EBVs) frameworks. Front. Mar. Sci. 5, 1. https://doi.org/10.3389/fmars.2018.00211. –15.

Muller-Karger, F.E., Hestir, E., Ade, C., Turpie, K., Roberts, D.A., Siegel, D., Miller, R.J., Humm, D., Izenberg, N., Keller, M., Morgan, F., Frouin, R., Dekker, A.G., Gardner, R., Goodman, J., Schaeffer, B., Franz, B.A., Pahlevan, N., Mannino, A.G., Concha, J.A., Ackleson, S.G., Cavanaugh, K.C., Romanou, A., Tzortziou, M., Boss, E.S., Pavlick, R., Freeman, A., Rousseaux, C.S., Dunne, J., Long, M.C., Klein, E., McKinley, G.A., Goes, J., Letelier, R., Kavanaugh, M., Roffer, M., Bracher, A., Arrigo, K.R., Dierssen, H., Zhang, X., Davis, F.W., Best, B., Guralnick, R., Moisan, J., Sosik, H.M., Kudela, R., Mouw, C.B., Barnard, A.H., Palacios, S., Roesler, C., Drakou, E.G., Appeltans, W., Jetz, W., 2018b. Satellite sensor requirements for monitoring essential biodiversity variables of coastal ecosystems. Ecol. Appl. 28, 749–760. https://doi.org/10.1002/eap.1682.

Phinn, S., Roelfsema, C., Dekker, A., Brando, V., Anstee, J., 2008. Mapping seagrass species, cover and biomass in shallow waters: an assessment of satellite multi-spectral and airborne hyper-spectral imaging systems in Moreton Bay (Australia). Remote Sens. Environ. 112, 3413–3425. https://doi.org/10.1016/j.rse.2007.09.017.

Poortinga, A., Tenneson, K., Shapiro, A., Nquyen, Q., Aung, K.S., Chishtie, F., Saah, D., 2019. Mapping plantations in Myanmar by fusing Landsat-8, Sentinel-2 and Sentinel-1 data along with systematic error quantification. Rem. Sens. https://doi.org/10.3390/rs11070831.

Poursanidis, D., Traganos, D., Reinartz, P., Chrysoulakis, N., 2019. On the use of Sentinel-2 for coastal habitat mapping and satellite-derived bathymetry estimation using downscaled coastal aerosol band. Int. J. Appl. Earth Obs. Geoinf. 80, 58–70. https://doi.org/10.1016/j.jag.2019.03.012.

Pu, R., Bell, S., 2017. Mapping seagrass coverage and spatial patterns with high spatial resolution IKONOS imagery. Int. J. Appl. Earth Obs. Geoinf. 54, 145–158. https://doi.org/10.1016/j.jag.2016.09.011.

Pu, R., Bell, S., Meyer, C., Baggett, L., Zhao, Y., 2012. Mapping and assessing seagrass along the western coast of Florida using Landsat TM and EO-1 ALI/Hyperion imagery. Estuar. Coast Shelf Sci. 115, 234–245. https://doi.org/10.1016/j.ecss.2012.09.006.

Pu, R., Bell, S., Meyer, C., 2014. Mapping and assessing seagrass bed changes in Central Florida's west coast using multitemporal Landsat TM imagery. Estuar. Coast Shelf Sci. 149, 68–79. https://doi.org/10.1016/j.ecss.2014.07.014.

Roelfsema, C., Kovacs, E.M., Saunders, M.I., Phinn, S., Lyons, M., Maxwell, P., 2013. Challenges of remote sensing for quantifying changes in large complex seagrass environments. Estuar. Coast Shelf Sci. 133, 161–171. https://doi.org/10.1016/j.ecss.2013.08.026.

Roelfsema, C.M., Lyons, M., Kovacs, E.M., Maxwell, P., Saunders, M.I., Samper-Villarreal, J., Phinn, S.R., 2014. Multi-temporal mapping of seagrass cover, species and biomass: a semi-automated object based image analysis approach. Remote Sens. Environ. 150, 172–187. https://doi.org/10.1016/j.rse.2014.05.001.

Roelfsema, C.M., Lyons, M., Murray, N., Kovacs, E.M., Kennedy, E., Markey, K., Borrego-Acevedo, R., Ordoñez Alvarez, A., Say, C., Tudman, P., Roe, M., Wolff, J., Traganos, D., Asner, G.P., Bambic, B., Free, B., Fox, H.E., Lieb, Z., Phinn, S.R., 2021. Workflow for the generation of expert-derived training and validation data: a view to global scale habitat mapping. Front. Mar. Sci. 8, 1–13. https://doi.org/10.3389/fmars.2021.643381.

Schrandt, M.N., MacDonald, T.C., Sherwood, E.T., Beck, M.W., 2021. A multimetric nekton index for monitoring, managing and communicating ecosystem health status in an urbanized Gulf of Mexico estuary. Ecol. Indicat. 123, 107310 https://doi.org/10.1016/j.ecolind.2020.107310.

Sherwood, E.T., Greening, H.S., Janicki, A.J., Karlen, D.J., 2016. Tampa Bay estuary: monitoring long-term recovery through regional partnerships. Reg Stud Mar Sci 4, 1–11. https://doi.org/10.1016/j.rsma.2015.05.005.

Sherwood, E.T., Greening, H.S., Johansson, J.O.R., Kaufman, K., Raulerson, G.E., 2017. Tampa Bay (Florida, USA): documenting seagrass recovery since the 1980's and reviewing the benefits. SE. Geogr. 57, 294–319. https://doi.org/10.1353/sgo.2017.0026.

Sudo, K., Quiros, T.E.A.L., Prathep, A., Luong, C Van, Lin, H.J., Bujang, J.S., Ooi, J.L.S., Fortes, M.D., Zakaria, M.H., Yaakub, S.M., Tan, Y.M., Huang, X., Nakaoka, M., 2021. Distribution, temporal change, and conservation status of tropical seagrass beds in Southeast Asia: 2000–2020. Front. Mar. Sci. 8, 1–11. https://doi.org/10.3389/fmars.2021.637722.

Telesca, L., Belluscio, A., Criscoli, A., Ardizzone, G., Apostolaki, E.T., Fraschetti, S., Gristina, M., Knittweis, L., Martin, C.S., Pergent, G., Alagna, A., Badalamenti, F., Garofalo, G., Gerakaris, V., Louise Pace, M., Pergent-Martini, C., Salomidi, M., 2015. Seagrass meadows (*Posidonia oceanica*) distribution and trajectories of change. Sci. Rep. 5, 1–14. https://doi.org/10.1038/srep12505.

Tomasko, D., Alderson, M., Burnes, R., Hecker, J., Leverone, J., Raulerson, G., Sherwood, E., 2018. Widespread recovery of seagrass coverage in Southwest Florida (USA): temporal and spatial trends and management actions responsible for success. Mar. Pollut. Bull. 135, 1128–1137. https://doi.org/10.1016/j.marpolbul.2018.08.049.

Tomasko, D.A., Corbett, C.A., Greening, H.S., Raulerson, G.E., 2005. Spatial and temporal variation in seagrass coverage in Southwest Florida: assessing the relative effects of anthropogenic nutrient load reductions and rainfall in four contiguous estuaries. Mar. Pollut. Bull. 50, 797–805. https://doi.org/10.1016/j.marpolbul.2005.02.010.

Topouzelis, K., Makri, D., Stoupas, N., Papakonstantinou, A., Katsanevakis, S., 2018. Seagrass mapping in Greek territorial waters using Landsat-8 satellite images. Int. J. Appl. Earth Obs. Geoinf. 67, 98–113. https://doi.org/10.1016/j.jag.2017.12.013.

Traganos, D., Reinartz, P., 2018. Mapping mediterranean seagrasses with sentinel-2 imagery. Mar. Pollut. Bull. 134, 197–209. https://doi.org/10.1016/j.marpolbul.2017.06.075.

Traganos, D., Aggarwal, B., Poursanidis, D., Topouzelis, K., Chrysoulakis, N., Reinartz, P., 2018. Towards global-scale seagrass mapping and monitoring using Sentinel-2 on Google Earth Engine: the case study of the Aegean and Ionian Seas. Rem. Sens. 10, 1–14. https://doi.org/10.3390/rs10081227.

Veettil, B.K., Ward, R.D., Lima, M.D.A.C., Stankovic, M., Hoai, P.N., Quang, N.X., 2020. Opportunities for seagrass research derived from remote sensing: a review of current methods. Ecol. Indicat. 117, 106560 https://doi.org/10.1016/j.ecolind.2020.106560.

Waycott, M., Duarte, C.M., Carruthers, T.J.B., Orth, R.J., Dennison, W.C., Olyarnik, S., Calladine, A., Fourqurean, J.W., Heck, K.L., Hughes, A.R., Kendrick, G.A., Kenworthy, W.J., Short, F.T., Williams, S.L., 2009. Accelerating loss of seagrasses across the globe threatens coastal ecosystems. Proc. Natl. Acad. Sci. U. S. A. 106, 12377–12381. https://doi.org/10.1073/pnas.0905620106.

Wicaksono, P., Wulandari, S.A., Lazuardi, W., Munir, M., 2021. Sentinel-2 images deliver possibilities for accurate and consistent multi-temporal benthic habitat maps in optically shallow water. Remote Sens Appl Soc Environ 23, 100572. https://doi.org/10.1016/j.rsase.2021.100572.

Wulder, M.A., White, J.C., Loveland, T.R., Woodcock, C.E., Belward, A.S., Cohen, W.B., Fosnight, E.A., Shaw, J., Masek, J.G., Roy, D.P., 2016. The global Landsat archive: status, consolidation, and direction. Remote Sens. Environ. 185, 271–283. https://doi.org/10.1016/j.rse.2015.11.032.

Yarbro, L.A., Carlson, P.R.J., 2016. Seagrass Integrated Mapping and Monitoring Program: Mapping and Monitoring Report No. 2. St. Petersburg, Florida, USA.

Zhang, L., Huang, X., Huang, B., Li, P., 2006. A pixel shape index coupled with spectral information for classification of high spatial resolution remotely sensed imagery. IEEE Trans. Geosci. Rem. Sens. 44, 2950–2961. https://doi.org/10.1109/TGRS.2006.876704.

Zoffoli, M.L., Gernez, P., Rosa, P., Le Bris, A., Brando, V.E., Barillé, A.L., Harin, N., Peters, S., Poser, K., Spaias, L., Peralta, G., Barillé, L., 2020. Sentinel-2 remote sensing of *Zostera noltei*-dominated intertidal seagrass meadows. Remote Sens. Environ. 251, 112020 https://doi.org/10.1016/j.rse.2020.112020.